JOURNAL OF VIROLOGY, Jan. 2005, p. 326–340 Vol. 79, No. 1
0022-538X/05/$08.00+0 doi:10.1128/JVI.79.1.326–340.2005

Role for Tumor Necrosis Factor Alpha in Murine Cytomegalovirus Transcriptional Reactivation in Latently Infected Lungs

Christian O. Simon, Christof K. Seckert, Doris Dreis, Matthias J. Reddehase,* and Natascha K. A. Grzimek

Institute for Virology, Johannes Gutenberg University, Mainz, Germany

Received 27 May 2004/Accepted 18 August 2004

Interstitial pneumonia is a major clinical manifestation of primary or recurrent cytomegalovirus (CMV) infection in immunocompromised recipients of a bone marrow transplant. In a murine model, lungs were identified as a prominent site of CMV latency and recurrence. Pulmonary latency of murine CMV is characterized by high viral genome burden and a low incidence of variegated immediate-early (IE) gene expression, reflecting a sporadic activity of the major IE promoters (MIEPs) and enhancer. The enhancer-flanking promoters MIEP1/3 and MIEP2 are switched on and off during latency in a ratio of ~2:1. MIEP1/3 latency-associated activity generates the IE1 transcript of the *ie1/3* transcription unit but not the alternative splicing product IE3 that encodes the essential transactivator of early gene expression. Splicing thus appeared to be an important checkpoint for maintenance of latency. In accordance with previous work of others, we show here that signaling by the proinflammatory cytokine tumor necrosis factor alpha (TNF-α) activates IE1/3 transcription in vivo. As an addition to current knowledge, Poisson distribution analysis revealed an increased incidence of IE1/3 transcriptional events as well as a higher amount of transcripts per event. Notably, TNF-α promoted the splicing to IE3 transcripts, but transcription did not proceed to the *M55/gB* early gene. Moreover, the activated transcriptional state induced by TNF-α did not predispose latently infected mice to a higher incidence of virus recurrence after hematoablative treatment. In conclusion, TNF-α is an important inductor of IE gene transcriptional reactivation, whereas early genes downstream in the viral replicative cycle appear to be the rate-limiting checkpoint(s) for virus recurrence.

Reactivation of latent cytomegalovirus (CMV) from donor or recipient tissues is a risk in solid organ transplantation as well as in bone marrow transplantation (BMT) (44). Interstitial pneumonia is a frequent manifestation of CMV disease with a high fatality rate after lung and heart-lung transplantation and after allogeneic BMT (6, 38, 54), suggesting that recurrent virus may directly originate from the lungs due to reactivating transcriptional signals induced by cellular stress conditions and/or cytokines associated with transplantation procedures and host-versus-graft or graft-versus-host immunological responses.

With this rationale, previous studies of the BALB/c (H-2^d haplotype) mouse model of CMV infection were focused on the lungs as an organ site of murine CMV (mCMV) pathogenesis (46, 53), immune control (3, 23, 24, 46, 53), establishment of latency (5, 19, 33, 35), transcriptional reactivation (34), and virus recurrence (34, 51, 59). Specifically, primary mCMV infection in the phase of hematopoietic reconstitution after hematoablative conditioning and experimental BMT resulted in a transient interstitial pneumonia that was resolved by newly reconstituted lung-infiltrating antiviral T cells (3, 24, 46). In vivo depletion of CD8 T cells, but not of CD4 T cells, during reconstitution led to a fatal disseminated viral pneumonia (46). This finding identified the CD8 T cells as the crucial antiviral effector cells in this experimental setting. Histologically, in the acute phase peaking at around 3 weeks after BMT, the CD8 T cells were found to confine the infection to inflammatory foci, and after 5 to 6 weeks, productively infected lung cells were no longer detectable. Notably, after full clinical convalescence from 2 months onward, a disseminated infiltrate consisting of activated L-selectin (CD62L)-negative CD8 T cells persisted in the lungs for the life span of the recipients (46), a finding that suggested iterative restimulation of these effector-memory cells by latency-associated viral antigen(s). A relative and absolute increase in the number of activated CD8 T cells specific for the major histocompatibility complex class I L^d-restricted, immediate-early protein 1 (IE1)-derived immunodominant peptide 168-YPHFMPTNL-176 (23) predicted the expression of the *ie1* gene in latently infected lung cells.

Molecular analysis verified the establishment of mCMV pulmonary latency. In the absence of infectivity measured by a high-sensitivity assay (35), the viral genome was found to be present in the lungs in a tissue load that varied between ~1,000 and 6,000 copies per 10^6 cells, depending on the extent and duration of productive infection which differ somewhat based on differences in reconstitution efficacies after BMTs (19, 33, 59). Most importantly, the incidence of virus recurrence induced by total-body γ-irradiation correlated with the latent genome load (59). In accordance with the immunological findings, correctly spliced, polyadenylated IE1 transcripts were detected in latently infected lungs (33), albeit in a very low number of transcriptional events reflecting a sporadic, variegated activity of the mCMV major IE (MIE) enhancer (14) and the MIE promoter MIEP1/3, which govern the *ie1/3* transcription unit (29, 42). The two enhancer-flanking promoters MIEP1/3 and MIEP2 were found to be active during pulmonary latency

* Corresponding author. Mailing address: Institute for Virology, Johannes Gutenberg University, Hochhaus am Augustusplatz, 55101 Mainz, Germany. Phone: 49-6131-39-33650. Fax: 49-6131-39-35604. E-mail: Matthias.Reddehase@uni-mainz.de.

independent of each other and in a pulse ratio of 2:1 (19). Contrary to the interpretation given previously by other investigators (21, 62), the expression of MIE genes did not indicate a low-level persistence of productive infection, often briefly referred to as persistence as opposed to latency. This became obvious from the absence of IE3 transcripts (33), the alternative splicing product of the *ie1/3* transcription unit. The IE3 protein is the mCMV homolog of human CMV (hCMV) IE2 (22; reviewed in reference 58), and, like hCMV IE2, it functions as an essential transactivator of early (E) gene expression (4). Accordingly, the E gene *M55* encoding glycoprotein B (gB) was found not to be expressed during latency (33). Splicing of IE3 thus appeared to be a molecular checkpoint for the maintenance of latency in the presence of MIEP activity.

MIE enhancers are very strong *cis*-acting regulatory elements composed of modules for transcription factor binding sites, including NF-κB binding sites (9, 14; for a review, see reference 18), and thus link MIE gene expression in infected cells with the cell's outside world in the context of normal, transplanted, or inflamed tissue. According to previous work of Stein et al. (60) and Prösch et al. (49) on the regulation of human CMV enhancer activity, the proinflammatory cytokine tumor necrosis factor alpha (TNF-α), the TNF ligand superfamily member 2, is known to activate IE gene expression via induction of NF-κB. This can occur along the TNF receptor type 1 (TNFR1)-TRADD-TRAF2-RIP-IκB kinase (IKK) or the TNFR2-TRAF2-RIP-IKK signaling pathway. In addition, by binding to TNFR1 as well as TNFR2 and recruitment of TRAF2, TNF-α can also activate AP1 via the MEKK1-MKK7-JNK pathway (for a recent review of TNF signaling pathways, see reference 2). Notably, the mCMV MIE enhancer is rich in potential AP1 binding sites (14), and work by Hummel et al. (26) has implicated both NF-κB and AP1 in the enhancement of mCMV *ie1* gene expression in the lungs of latently infected mice after intravenous administration of recombinant murine TNF-α. However, TNF-α in cooperation with gamma interferon induces an antiviral state in pretreated cells that is operative at the stage of nucleocapsid maturation (39). During an ongoing infection, mCMV gene functions induce resistance to TNF-α by downmodulation of TNF receptors (48). Both mechanisms argue against the proposed enhancement of virus recurrence by TNF-α.

Here, we used the established model of mCMV latency in the lungs after experimental BMT to address the pending question of whether TNF-mediated in vivo activation of MIE transcription can override the IE3 splicing checkpoint of latency and initiate the productive viral cycle for virus recurrence.

MATERIALS AND METHODS

Experimental BMT and establishment of latent mCMV infection. Sex-matched syngeneic BMT with female BALB/c (H-2^d haplotype) mice as bone marrow cell donors and recipients was performed as described previously (45). In brief, hematoablative conditioning of 8- to 9-week-old recipients was achieved by total-body γ-irradiation with a single dose of 6 Gy. BMT was performed 6 h later by infusion of 5×10^6 femoral and tibial donor bone marrow cells into the tail vein of the recipients. At ca. 2 h after BMT, recipients were infected with 10^5 PFU of mCMV (strain Smith ATCC VR-1399, purchased in 1981 as strain Smith ATCC VR-194) in the left hind footpad. Criteria for the definition of latency were specified previously (for a review, see reference 52) and include the absence of infectivity in key organs of CMV tropism (spleen, lungs, and salivary glands) as well as PCR-verified absence of viral DNA from blood (<1 copy per 10^4 leukocytes). For this experiment, the decline of viral DNA load in blood taken from the tail vein was monitored for individual recipients in monthly intervals until the detection limit was reached. It should be noted that the cessation of productive infection in organs precedes clearance of viral DNA from the intravascular compartment by several months (35; reviewed in reference 52). In the reported experiments, analyses were performed at 12 months after BMT and infection. Animals were bred and housed in the central animal facility of the Johannes Gutenberg University under specified pathogen-free conditions, and animal experiments were approved according to German federal law under permission number 177-07/021-28.

Administration of TNF-α. Latently infected mice were injected into the tail vein with 0.25 or 1 μg of recombinant murine TNF-α (catalog no. 410-MT-050; R&D Systems) in 0.5 ml of physiological saline. The dose was lower than the 2.5 μg used intravenously (i.v.) in the experiments reported by Hummel et al. (26), because we observed a high lethality within 24 h after administration of 2.5 μg. It should be noted that this difference between the protocols is not a discrepancy because the systemic toxicity of TNF-α (systemic inflammatory response syndrome) is known to be attenuated by preceding infections and thus depends on the hygiene status of the animal facility. At 24 h after infusion of TNF-α or of physiological saline in the control group, mice were either γ-irradiated with a dose of 6.5 Gy for the induction of virus recurrence or sacrificed for transcriptional analysis (see below).

Construction of a recombinant plasmid standard for viral DNA quantification. Plasmid pDrive_gB_PTHrP_Tdy, which contains sequences of mCMV *M55/gB* as well as sequences of the cellular genes *pthrp* (mouse parathyroid hormone-related peptide-encoding gene) (40) and *tdy* (male sex [testes]-determining gene) (20), was constructed as follows. Plasmid pDrive_gB was generated as a first intermediate. For this, a fragment of the *gB* gene was amplified from mCMV virion DNA by PCR using oligonucleotides gB-forw (5′-TGTACAAGT GAGGTAATCGCGG-3′) and gB-rev (5′-TATTATTATCCTCGCAGCGTCT CC-3′) as forward and reverse primers, respectively. The 2,817-bp amplification product, representing the mCMV *gB* sequence from map positions 82,910 to 85,726 (GenBank accession no. NC_004065 [complete genome]) (50), was cloned into pDrive by means of UA-based ligation (catalog no. 231122; QIAGEN, Hilden, Germany). Plasmid pDrive_gB_PTHrP was generated as a second intermediate. For this, a 984-bp *gB* fragment within pDrive_gB was deleted by ApaI and XbaI digestion. Primers PTHrP-7 (5′-TATAGGGCCCGC TGTGTCTGAACATCAGCT-3′ [the ApaI site is underlined]) and PTHrP-8 (5′-TTAATCTAGACTTTGTACGTCTCCACCTTG-3′ [the XbaI site is underlined]) served to amplify a 238-bp *pthrp* fragment from cellular DNA isolated from mouse tail tissue (DNeasy tissue kit, catalog no. 69504; QIAGEN). A 258-bp amplification product containing the 238-bp *pthrp* sequence from map positions 126 to 363 (GenBank accession no. M60056) was digested with ApaI and XbaI and inserted into ApaI- and XbaI-digested pDrive_gB. For the final construction of pDrive_gB_PTHrP_Tdy, pDrive_gB_PTHrP was linearized by ApaI cleavage and ligated into a 407-bp fragment encompassing the 401-bp sequence of *tdy* representing map positions 70 to 470 (GenBank accession no. 287804). This fragment was generated by PCR by using cellular DNA from male mouse tail tissue as a template and ApaI site-containing oligonucleotides Tdy-forw (5′-AAAAGGGCCCTGGGACTGGTGACAATTGTC-3′) and Tdy-rev (5′-AAAAGGGCCCAGTACAGGTGTGCAGCTCTAC-3′) (the ApaI sites are underlined) as forward and reverse primers, respectively. For use as a standard template in real-time PCR (see below), pDrive_gB_PTHrP_Tdy was linearized by digestion with SmaI. Enzyme reactions were performed as recommended by the suppliers. For a map of pDrive_gB_PTHrP_Tdy, see Fig. 2A.

Quantitation of latent viral genome in lung tissue. Lung tissue derived from the postcaval lobe (representing a 1/9 portion of the lungs with ca. 6×10^6 to 7×10^6 cells) was minced, and DNA was extracted with the DNeasy tissue kit (catalog no. 69504; QIAGEN) as described in the manufacturer's DNeasy tissue handbook (manual no. 05/2002) protocol for animal tissues. In brief, samples were lysed by proteinase K digestion followed by DNA binding to the DNeasy mini column, washing steps, and two rounds of DNA elution with 100 μl of the elution buffer yielding 20 to 30 μg of DNA in a total volume of 200 μl. Latent viral genomes were quantitated by real-time PCR using the LightCycler system (Roche, Mannheim, Germany) and the QuantiTect SYBR Green PCR kit (catalog. no. 204143; QIAGEN). A 100-ng aliquot of the lung DNA was added as template DNA to reaction capillaries containing a reaction mixture that included 2× QuantiTect SYBR Green PCR master mix with an initial $MgCl_2$ concentration of 2.5 mM and 1 μM each primer. Primers for amplification of the 135-bp fragment of the viral gene *M55/gB* were LCgB-forw (5′-GAAGATCCGCATG TCCTTCAG-3′) and LCgB-rev (5′-AATCCGTCCAACATCTTGTCG-3′), representing map positions 84,017 to 84,037 and 84,151 to 84,131, respectively

(GenBank accession no. NC_004065 [complete genome]). Primers for amplification of a 142-bp fragment of the *pthrp* gene were LCPTHrP-forw (5′-GGTA TCTGCCCTCATCGTCTG-3′) and LCPTHrP-rev (5′-CGTTTCTTCCTCCAC CATCTG-3′), representing map positions 327 to 307 and 186 to 206, respectively (GenBank accession no. M60056). PCR was performed with the following cycler conditions: an initial step of 15 min at 95°C for HotStarTaq DNA polymerase activation followed by 50 cycles of 15 s at 94°C, 30 s at 62°C, and 15 s at 72°C. Data were obtained during the extension period in the "single mode." After amplification, melting curve analysis of the PCR products was performed by raising the temperature to 98°C, cooling down rapidly to 65°C for 15 s, and then slowly (0.1°C/s) raising the temperature again to 94°C, with the fluorescence being recorded continuously. Lung DNA samples of ca. 100 ng were tested in triplicate. Standard curves for quantification were established by using graded numbers of linearized plasmid pDrive_gB_PTHrP_Tdy as a template. The PCR amplification efficiencies (E) for the *M55/gB* and *pthrp* standard curves as well as for both genes in a titration of sample DNA were calculated according to the formula $E = 10^{-1/\text{slope}}$ (technical note no. LC11/2000; Roche Molecular Biochemicals) and differed by $\Delta E < 0.05$ in the reported experiments. Likewise, for each of the two genes tested, amplification efficacies differed by $\Delta E < 0.05$ between a titration of sample DNA and the respective standard curve.

High-sensitivity assay for viral infectivity. The absence of infectious virus in latently infected lungs was verified and virus recurrence was monitored by the reverse transcription (RT)-PCR-based "focus expansion assay " capable of detecting 0.01 PFU representing five copies of the viral genome (35; reviewed in reference 52). The test was performed essentially as described previously (35), except that shock-frozen tissue was homogenized in a QIAGEN Mixer Mill MM300 at 30 Hz for 2.5 min with a steel ball (0.118 in.) in 1.5 ml of culture medium. After centrifugal (1,000 × *g* for 30 min at 20°C) inoculation of highly permissive mouse embryofetal fibroblast indicator cells (45) with the tissue homogenate in an appropriate dilution (35), viral replication was allowed to proceed for 72 h, mRNA was purified from the indicator cells by using a QuickPrepMicro mRNA purification kit (catalog. no. 27-9255-01; Amersham Biosciences), and RT-PCR specific for IE1 transcripts was performed. Amplification products were analyzed by agarose gel electrophoresis, Southern blotting, and hybridization of the 188-bp amplificate with the γ-^{32}P-end-labeled probe IE1-P directed against the *ie1/3* exon 3-exon 4 splice junction (19), followed by autoradiography.

Isolation of poly(A)$^+$ RNA from the lungs. Shock-frozen lung pieces, each representing a 1/18 portion of the lungs, were transferred without delay to Eppendorf tubes (one piece per tube) containing 900 μl of high-salt lysis-binding buffer (μMACS mRNA isolation kit no. 130-075-201; Miltenyi Biotec, Bergisch Gladbach, Germany) and a steel ball (0.118 in.). Pieces were homogenized with a QIAGEN Mixer Mill MM300 at 30 Hz twice for 3 min and interrupted by rotation of the Mixer Mill rack to allow even homogenization. Poly(A)$^+$ RNA was isolated as recommended by the supplier by binding to paramagnetic oligo(dT) MicroBeads in μMACS type columns, except that the washing steps with wash buffer were followed by digestion of contaminating DNA. For this process, 100 μl of a DNase mix consisting of 5 μl of DNase (catalog. no. 27-0514-02; Amersham Biosciences) and 95 μl of assay buffer (40 mM Tris-HCl [pH 7.5], 6 mM $MgCl_2$) was applied, and columns were incubated for 10 min at 20 to 25°C. The reaction was blocked by rinsing the column two times with 150 μl of stop solution (2 mM EGTA in lysis-binding buffer). After further washing steps, the retained poly(A)$^+$ RNA was eluted under maintenance of the magnetic field with 120 μl of elution buffer preheated at 65°C. The first drop was discarded, and the second to fourth drops were collected. Collected samples were adjusted to a volume of 75 μl with RNase-free water and stored at −70°C. The absolute yield was found to be ~2 μg per lung piece. According to the manufacturer, the relative yield is ca. 70% when tested with 1 μg of 3′-labeled poly($A_{n=120}$)$^+$ RNA (Miltenyi Biotec product specialists). Therefore, the loss of poly(A)$^+$ RNA in the columns is practically negligible.

Analysis and quantitation of transcripts. Transcripts of the viral genes *m123/ie1*, *M122/ie3*, and *M55/gB* (50) were detected by specific RT-PCRs, for which all primers and probes were described previously (19, 33), yielding amplificates of 188, 229, and 405 bp, respectively. One-step RT-PCR was performed as recommended by the manufacturer (OneStep RT-PCR kit handbook manual no. 05/2002; QIAGEN) and carried out by using 96-well reaction plates (MicroAmp Optical; Applied Biosystems, Foster City, Calif.) with a GeneAmp 5700 thermocycler (Perkin-Elmer). The poly(A)$^+$ RNA test samples represented 1/10 of the yield from one lung tissue piece (see above), usually ~200 ng. Standard titrations for quantitation were established with in vitro transcripts synthesized and purified as specified previously (33). For this, RT-PCRs were performed with defined graded numbers of synthetic test RNA molecules and 4 μg of poly(A)$^+$ carrier RNA (from a High Pure viral nucleic acid kit, catalog no. 1858874; Roche) added to the reaction mix in a volume of 1 μl.

For IE1 and IE3 transcripts, the reaction was performed with a total volume of 25 μl containing 5 μl of 5× QIAGEN OneStep RT-PCR buffer, 1 μl of QIAGEN OneStep RT-PCR enzyme mix, 800 μM each deoxynucleoside triphosphate, 0.6 μM each primer, additional $MgCl_2$ to adjust the concentration to 3.74 mM, and 7.5 μl of the poly(A)$^+$ RNA specimen. RT was performed for 30 min at 50°C. Cycler conditions for the amplification of the resulting cDNA were as follows: an initial activation step for the HotStarTaq DNA polymerase for 15 min at 95°C followed by 33 cycles consisting of a denaturation step at 94°C for 30 s, a primer-annealing step at 58°C for 1 min, and an elongation step at 72°C for 1 min that was extended to 10 min in the last cycle. For the M55/gB transcript, the reaction mix was the same as that specified above except that the primer concentration was 0.3 μM and the additional $MgCl_2$ was 0.62 μM. The cycler protocol for cDNA amplification involved an initial activation step for 15 min at 95°C followed by 35 cycles of denaturation at 95°C for 10 s and combined primer-annealing and elongation step at 50°C for 1 min. The reaction was concluded by a final elongation at 72°C for 5 min. In some experiments, 1 μg of template poly(A)$^+$ RNA present in 37.5 μl was accommodated by upgrading the total reaction volume to 75 μl.

Amplification products were analyzed by agarose gel electrophoresis, Southern blot, and hybridization with the γ-^{32}P-end-labeled probe IE1-P (*ie1/3* exon 3-exon 4 splice junction), IE3-P (*ie1/3* exon 3-exon 5 splice junction), and gB-P (19, 33). Signals were visualized by autoradiography. For quantitation, radioactivity was measured as phosphorstimulated luminescence units by digital phosphorimaging (Fujifilm bioimaging system BAS 2500; Fuji, Tokyo, Japan) using Tina 2.10 software (Raytest, Straubenhardt, Germany) for data analysis.

Frequency estimation of transcriptional events in lung tissue. Lungs were cut into 18 bona fide equally sized pieces. Pieces referred to as pieces 1 to 3, 4 to 6, and 7 to 9 were derived from the superior, middle, and inferior lobes of the right lung, respectively. Pieces 10 and 11 were derived from the postcaval lobe, and pieces 12 to 18 were derived from the left lung. The presence of transcripts was tested piece by piece, usually for a total of 90 pieces derived from the lungs of five mice per experimental group. Previous work on latency-associated (19, 33) and reactivation-associated (34) transcription in the lungs has shown that transcriptional events are generally so rare that a resolution defined by 18 experimental pieces per lung is sufficient to yield "on-or-off" patterns with transcriptionally active (on, positive) and transcriptionally silent (off, negative) pieces. This fact allows the performance of a Poisson distribution analysis (see reference 36) for estimating the frequency of transcriptional events by a reverse limiting dilution approach from the fractions of negative pieces $f(0)$ among 18 experimental pieces as well as among 9 (2 experimental pieces combined), 6 (3 experimental pieces combined), and 3 (6 experimental pieces combined) virtual pieces (described in greater detail in the appendix of reference 19). Most probable numbers (MPN), P values for the null hypothesis (goodness of fit, that is, conformity to the Poisson law), and the 95% confidence intervals (CI) for the MPN were calculated on the basis of the Poisson distribution equation $\lambda = 1/\text{MPN} = -\ln f(0)$ by using the maximum-likelihood method (15) as well as the minimum chi-square method (61). As both methods gave essentially the same results, data are shown for the calculation with the maximum-likelihood method only. The fraction of pieces containing n ($n = 0, 1, 2, 3$, and so forth) transcriptional events, $F(n)$, was calculated by the formula $F(n) = \lambda^n \times e^{-\lambda}/n!$ (factorial), which gives $F(0) = e^{-\lambda}$ for $n = 0$ and $F(n) = \lambda/n \times F(n-1)$ for $n > 0$. The estimates were based on experimental data from 90 pieces derived from the lungs of five mice and were then downextrapolated to 18 pieces of a representative, prototypical lung. Since the number of transcriptional events is always an integer, calculated decimals were rounded up or down appropriately according to the rule of least difference.

RESULTS

Design and flow of the experiments. A flow chart of the experiments is shown in Fig. 1. Sex-matched syngeneic BMT was performed with female BALB/c mice as bone marrow cell donors and recipients. Shortly after BMT, recipients were infected with mCMV. In this experimental setting, productive infection was controlled by hematopoietically reconstituted, tissue-infiltrating CD8 T cells (24, 46). Progressive clearance of viral DNA from the blood was monitored by real-time quantitative PCR until the detection limit was reached (data not

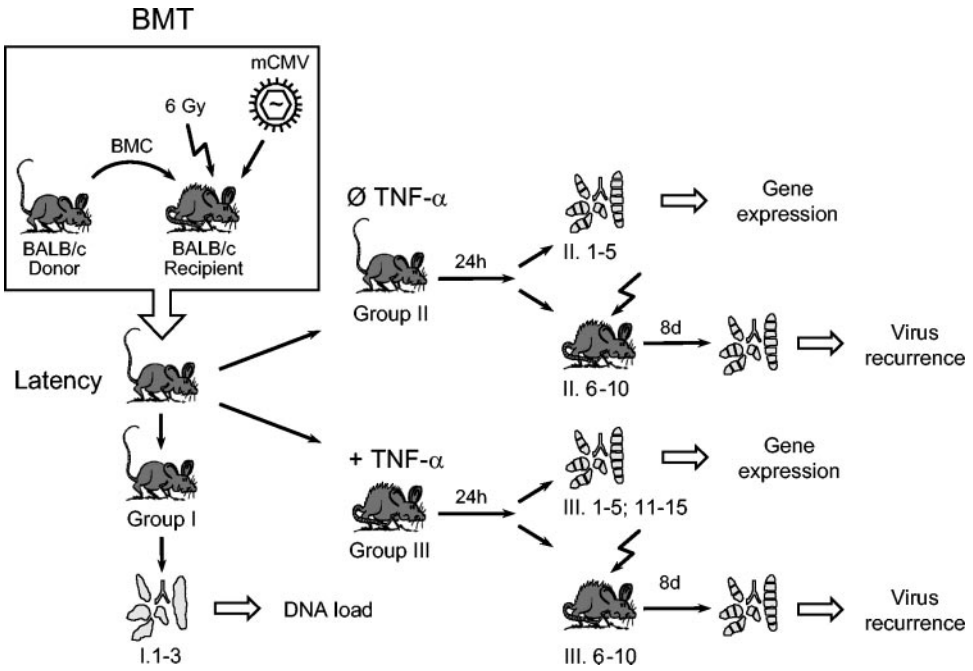

FIG. 1. Experimental regimen and time course. Syngeneic BMT was performed with BALB/c mice as donors and recipients by transplantation of donor bone marrow cells (BMC) to recipients γ-irradiated with a dose of 6 Gy. The BMT recipients were infected with mCMV, and the clearance of productive infection was monitored longitudinally by means of declining viral DNA load in the tail vein blood until the PCR detection limit was reached. Latency analyses were performed 1 year after primary infection. The latently infected BMT recipients were randomized to form three groups. Group I was used to determine the latent viral DNA load in the lungs. Groups II and III were compared to determine the effect of TNF-α on latency-associated viral gene expression and on the incidence of virus recurrence after secondary hematoablative γ-irradiation with a dose of 6.5 Gy. Both parameters were measured for 18 pieces per lung to facilitate frequency estimates by Poisson distribution statistics. The clinical health status of the mice is symbolized. For further details, see the text.

shown; reviewed in reference 52). Analyses of viral latency were performed at 12 months after BMT. The latently infected BMT recipients were randomized and subdivided into three experimental groups. Group I (mice I.1 to I.3) served to determine the load of latent viral DNA in the lungs. Group II (mice II.1 to II.10) was used to study latency-associated viral transcription (mice II.1 to II.5) as well as inducible virus recurrence (mice II.6 to II.10). Finally, group III (mice III.1 to III.15) was used to determine the influence of TNF-α on viral transcription (mice III.1 to III.5 and III.11 to III.15 for 1 and 0.25 μg of TNF-α, respectively) as well as on inducible virus recurrence (mice III.6 to III.10 for 1 μg of TNF-α).

Viral DNA load in latently infected lungs. Previous work with the same experimental model has shown that the lungs are an organ site of mCMV latency and that the viral DNA load in lung tissue varies depending upon the magnitude and duration of acute productive infection, which in turn depends on the efficacy of the hematopoietic reconstitution of protective CD8 T cells (59). Since the probability of reactivation is a function of the number of latent viral genomes (59), it is of predictive value to know the viral DNA load for each BMT-mCMV latency experiment. In previous work by Kurz et al. (33), the latent viral genomes were found to be more or less evenly distributed in the lungs, ranging between ~6,000 and 9,000 copies per 10^6 cells in individually tested pieces of lung tissue. The load was slightly lower in the work by Grzimek et al. (19), ranging between 3,000 and 6,800 copies per 10^6 cells in the lungs of five latently infected mice tested individually.

In the work by Steffens et al. (59), substitution of BMT with 10^6 antiviral CD8 T cells reduced the load from 5,000 copies to 1,000 copies per 10^6 cells. Here, we have employed real-time quantitative PCR to determine the viral DNA load in the postcaval lung lobes of mice I.1 to I.3, selected randomly from the latently infected BMT recipients (Fig. 2).

Plasmid pDrive_gB_PTHrP_Tdy (Fig. 2A) was constructed to serve as a common standard for a viral gene, *M55*/*gB*, the autosomal single-copy cellular gene *pthrp* (two copies in the diploid set of chromosomes), and the heterosomal male sex-determining gene *tdy*. It should be noted that *tdy* was not utilized in this report but was included in the tool for future studies on mCMV infection in sex-mismatched models of BMT to allow for a distinction between donor-derived and recipient-derived cells. The latent viral DNA load in the lungs was found to be in the order of 2,000 copies per 10^6 lung cells (i.e., per 2×10^6 copies of *pthrp*), with only little variance between the three mice tested (Fig. 2B and C). In conclusion, compared with the previous reports cited above, the load was fairly low in this group of latently infected BMT recipients and thus predicted a low incidence of inducible virus reactivation and recurrence.

Sensitivity and sampling error in the detection of IE1 transcripts. As was shown by previous work (19, 33), spliced IE1 transcripts representing exons 1 to 4 of the *ie1*/*3* transcription unit can be detected in latently infected lungs. This latency-associated transcription, though, was a rare event reflecting transgene-like variegated expression (16). Specifically, when

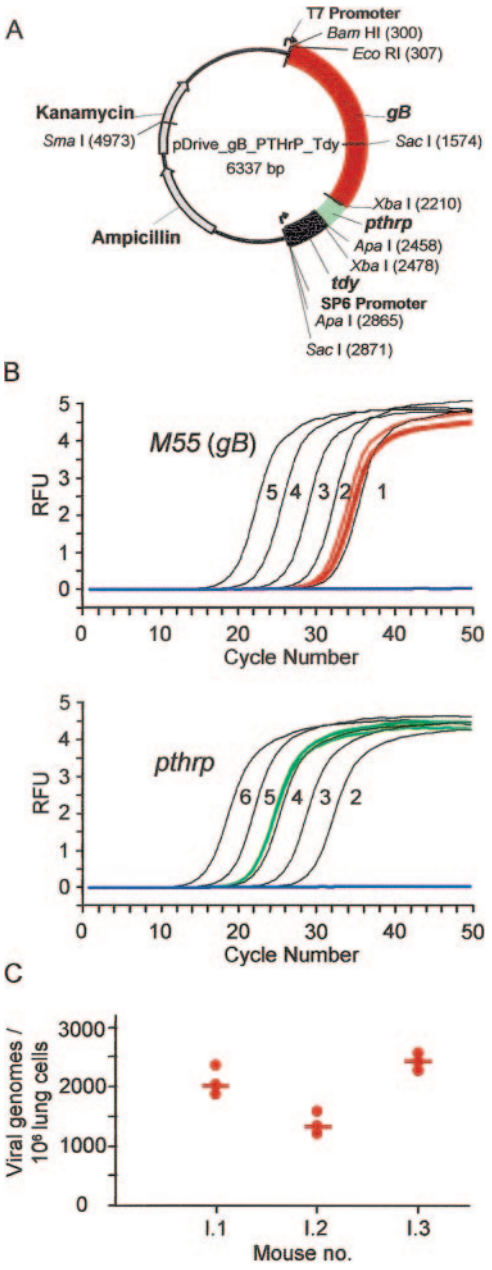

FIG. 2. Viral DNA load in latently infected lungs. (A) Physical map of plasmid pDrive_gB_PTHrP_Tdy that was constructed to serve as a standard in LightCycler real-time PCR. It encompasses the mCMV gene *M55/gB* (red) as well as the cellular genes *pthrp* (green) and *tdy* (black). (B) Amplification profiles for 10^1 to 10^6 copies (labeled by exponents 1 to 6, respectively) of the linearized standard plasmid and of a triplicate sample of lung DNA. A control containing all reaction components except sample DNA (water control) is shown in blue. At a glance, ~10 copies of the viral gene *M55/gB* (red) correspond to ~10,000 copies of the cellular gene *pthrp* (green). RFU, relative fluorescence units. (C) Viral DNA load determined individually for the lungs of the three mice of group I. Each red dot represents the mean value of a sample DNA triplicate determined with one standard curve. As DNA quantitation is subject to error, the determination was repeated three times with independent standard curves and independent DNA measurements for the sample DNA. The median values are marked by red horizontal bars.

the lungs were cut into 18 equally sized pieces in the so-called "mosaic approach" for in situ transcriptional analysis (33), an on-or-off pattern was observed with tissue pieces positive or negative for IE1 transcripts, respectively. Per definition, a positive tissue piece must contain at least one transcriptional event, that is, a minimum of one transcriptionally active viral genome. To define such an event in quantitative terms, it is important to determine the sensitivity of the RT-PCR, which depends primarily on the efficacy of reverse transcription. For this determination, synthetic poly($A_{n\ =\ 30}$)$^+$-IE1 transcripts were serially diluted in duplicate, each independent dilution series starting with 10^3 molecules. The detection limit was reached at eight transcripts in the first titration and at four transcripts in the second (Fig. 3A), which indicated a sampling error resulting in positive and negative samples due to Poisson distribution statistics (36) becoming effective at around eight molecules. Based on this preinformation, a detailed limiting dilution analysis was performed with 12 replicates per dilution to determine the fractions of negative replicates (Fig. 3B). By using the maximum-likelihood method (15), the number of transcripts for which a 1/e (~0.37) fraction of samples (Poisson distribution parameter, $\lambda = 1$) scored negative was estimated to be 3.5 with a 95% confidence interval of 2.3 to 5.3 (Fig. 3C).

As our decision on positive transcription in a lung tissue piece is experimentally based on the analysis of a 1/10 aliquot of the yield of poly(A)$^+$ RNA, a transcriptional event is statistically defined by the presence of 35 transcripts in the whole tissue piece. However, to avoid any underestimation by sampling error, the fraction of negative samples $f(0)$ must be $<1/10$. According to the Poisson distribution equation λ limit $= -\ln f(0) = -\ln 0.1 = 2.3$, a transcriptional event scores positive in 10 of 10 aliquots of the yield of poly(A)$^+$ RNA only if $>2.3 \times 35 = 80$ transcripts are present in the tissue piece. The optimal sensitivity can be exploited only if the material is used up, but this precludes further experiments. In the subsequent transcriptional analyses, a transcriptional event is operationally defined by a positive signal in a single 1/10 aliquot. Therefore, frequencies of transcriptional events have to be taken as minimum estimates.

TNF-α raises the frequency of detectable transcriptional events in a linear dose-dependent manner. Based on a time schedule established by Hummel et al. (26), which had revealed a response optimum at 24 h, the impact of soluble recombinant murine TNF-α on IE1 transcription in the lungs of latently infected BMT recipients was tested 24 h after a single intravenous injection. According to the mosaic approach discussed above, the lungs were cut into 18 pieces. IE1-specific RT-PCR was performed piece by piece for 90 pieces derived from the lungs of mice II.1 to II.5 and for 90 pieces derived from the lungs of mice III.1 to III.5, representing the basal and the TNF-induced IE1 transcription, respectively (Fig. 4A). Basal transcriptional activity was detected in the lungs of each of the five mice tested but in only a few lung tissue pieces, 10 out of 90 pieces altogether. This incidence of basal IE1 transcription was thus somewhat lower than that reported in previously published experiments (19, 33), which may relate to the lower number of latent viral template genomes (see above). While most of the positive pieces contained an amount of transcripts close to the detection limit, piece 12 from mouse II.3 and piece 16 from mouse II.4 showed a fairly high tran-

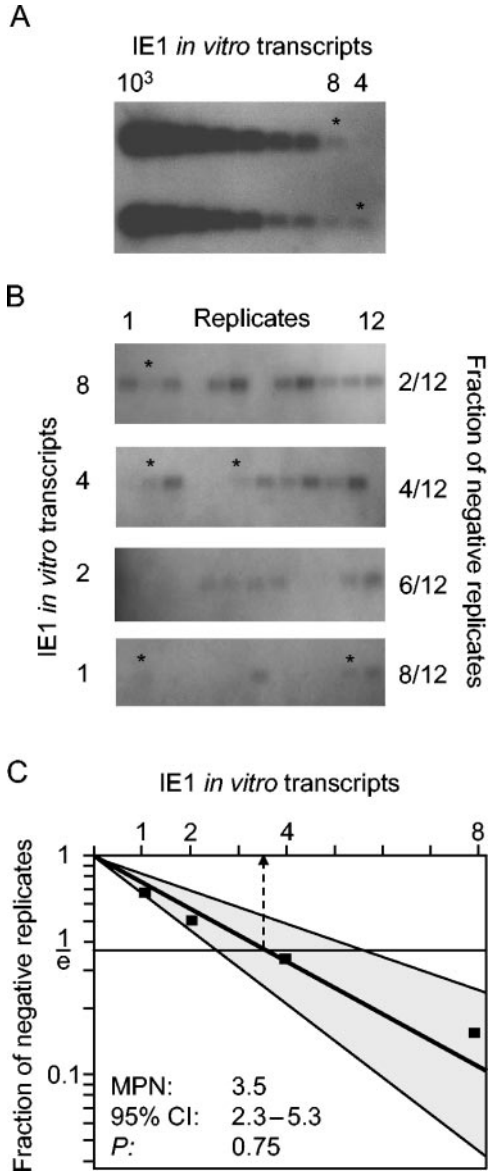

FIG. 3. Sensitivity of the IE1-specific RT-PCR. (A) Two independent titrations of IE1 in vitro transcripts. Shown are Southern blot autoradiographs of 188-bp cDNA amplificates after hybridization with the γ-^{32}P-end-labeled probe IE1-P that is directed against the exon 3-exon 4 splicing junction of transcription unit *ie1/3*. Titration end points are marked by asterisks. (B) Limiting dilution of IE1 in vitro transcripts in 12 replicates per indicated copy number. Asterisks mark faint signals, which are visible on the original roentgen film. (C) Limiting dilution graph showing the intercept-free linear regression line and its 95% CI (shaded area), calculated by the maximum-likelihood method. Based on Poisson distribution statistics, the MPN is the abscissa coordinate (dashed arrow) of the point of intersection between 1/e and the regression line. *P*, probability value indicating the goodness of fit.

scriptional activity, which is a reflection of the previously reported phenomenon of variegation of latency-associated transcription (for a review, see reference 52). At a glance, a stimulus by 1 μg of TNF-α markedly increased the number of positive pieces to 58 out of 90 altogether. Notably, in many instances, transcriptionally silent pieces were located next to pieces with very high transcription, which reconfirms our previous conclusion that the on-or-off phenomenon is not just a detection limit problem but indeed reflects the presence and absence of transcriptional events, also referred to as foci of transcription (33). Since a positive piece may of course contain more than one transcriptional focus, the number of transcriptional foci exceeds the number of experimentally observed positive pieces. The Poisson law is the statistical tool for calculating the frequency of transcriptional foci from the fraction of negative pieces (see the appendix in reference 19). Figure 4B shows the conformity to the Poisson distribution, as indicated by a log-linear function, and the difference in the frequencies of transcriptional events between experimental groups II and III. Specifically, 11 foci with a 95% confidence interval of 8 to 16 foci were calculated for the basal activity in the five mice of group II, whereas 93 foci with a 95% confidence interval of 76 to 114 foci were calculated for the TNF-induced activity in the five mice of group III. Figure 4C summarizes these data and includes the results for mice III.11 to III.15, which had received 0.25 μg of TNF-α. As expected, this lower dose resulted in a lower cumulative frequency, namely, in 34 foci with a 95% confidence interval of 27 to 43 foci. Interestingly, there is a linear relation between the dose of the inducing cytokine and the number of transcriptional events. It should be noted that systemic toxicity of murine TNF-α (10) precluded the testing of higher doses. In conclusion, TNF-α stimulates IE1 transcription from latent mCMV genomes in vivo and thereby increases the incidence of transcriptional events in the lungs of latently infected mice.

TNF-α raises the amount of transcripts present within transcriptional foci. The Poisson distribution predicts a range of one to four transcriptional events to be present in the positive pieces of the TNF-induced group III (see the legend of Fig. 9 for an explanation). The differences in signal strengths, however, appeared to be higher than just fourfold (Fig. 4A). This visual impression also suggested an influence of TNF-α on the rate of transcription per transcriptional event. For experimental verification, appropriate aliquots of purified poly(A)$^+$ RNA were pooled from the 10 positive pieces from mice II.1 to II.5 of group II, representing 11 foci, and from the 58 positive pieces from mice III.1 to III.5 of group III, representing 93 foci. For the two pools, IE1-specific RT-PCR was performed with a serial dilution of the poly(A)$^+$ RNA that started with a 1/100 aliquot of the yield normalized to 10 foci (Fig. 5A).

Relative quantitation by phosphorimaging revealed a 16-fold-higher amount of transcripts per transcriptional focus in the TNF-induced group (Fig. 5B). An estimation of the absolute number of transcripts per focus was obtained by using graded numbers of synthetic IE1 transcripts for a standard curve. As shown in Fig. 5C, a 1/100 aliquot of 10 foci contains 4 and 64 transcripts, which is 40 and 640 transcripts per focus for mice II.1 to II.5 and III.1 to III.5, respectively.

Altogether, increases in focus number and number of transcripts per focus combined, signaling by 1 μg of TNF-α enhanced the in situ IE1 transcription in latently infected lungs by a factor of ~135.

TNF-α promotes the generation of IE3 transcripts but not of downstream E gene transcripts. The absence of spliced IE3 transcripts specifying the essential transactivator of E-phase gene expression was a molecular hallmark of latency-associ-

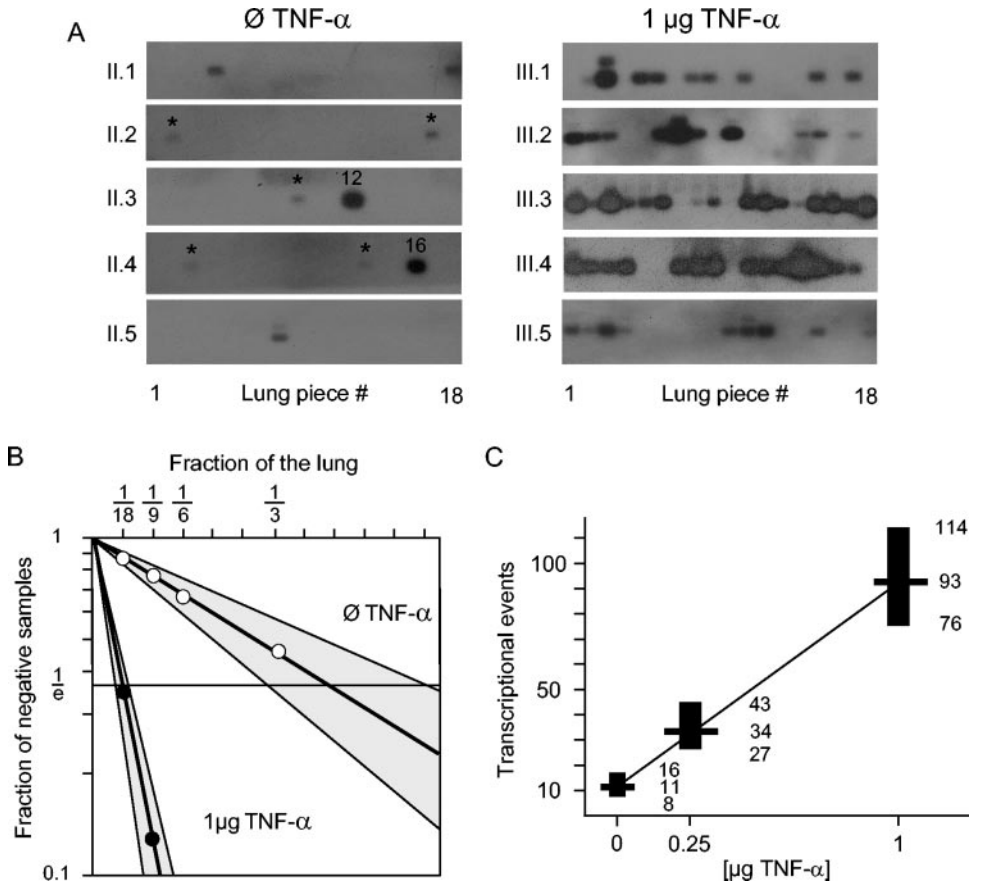

FIG. 4. Effect of TNF-α on the frequency of IE1-specific transcription in latently infected lungs. (A) Lungs were subdivided into 18 pieces, and IE1-specific RT-PCR was performed with poly(A)$^+$ RNA isolated from the individual pieces. Basal latency-associated IE1 transcription was tested for five mice of group II (left panel) and induced IE1 transcription was tested for five mice of group III (right panel) 24 h after i.v. infusion of saline (Ø TNF-α) and of 1 μg of recombinant murine TNF-α, respectively. Shown are the Southern blot autoradiographs after hybridization with probe IE1-P. Asterisks mark faint signals that are visible on the original roentgen film. The fraction of signal-negative pieces is the information that enters the Poisson distribution analysis. (B) Limiting dilution graphs showing the linear regression lines with the 95% confidence intervals (shaded areas) for the frequency of basal expression (Ø TNF-α, open circle; $P = 0.99$) and of TNF-induced expression (1 μg of TNF-α, closed circle; $P = 0.94$). (C) Graph illustrating the linear relation between the number of transcriptional events or foci and the dose of TNF-α, including the results for 0.25 μg of TNF-α obtained with mice III.11 to III.15. The number of transcriptional events refers to the 90 lung tissue pieces altogether of all five lungs tested per group. Most probable numbers, as derived from the limiting dilution analyses in panel B, are indicated by horizontal bars, and the extensions of the vertical bars represent the 95% confidence intervals. As a reading example, the lungs of mice III.1 to III.5 altogether contained 93 foci of IE1 transcription within 90 pieces, with a predicted variance of between 76 and 114 foci.

ated MIE transcription that explained the maintenance of latency and defined a second latency checkpoint operative after MIE *ie1/3* transcription initiation (33). It was therefore of interest to test whether the TNF-induced enhancement of MIE gene transcription is restricted to the generation of IE1 transcripts or whether TNF-α leads to a full reactivation of the viral transcriptional program (Fig. 6). For this test, the assay sensitivity was improved by upgrading the RT-PCRs to accommodate 1 μg of poly(A)$^+$ RNA pooled from the 58 lung tissue pieces that had scored positive for IE1 transcripts. This amount of template represented a 1/100 aliquot of 80 IE1-defined transcriptional events containing ~500 IE1 transcripts (see the calculation above). Notably, IE3 transcripts were detected in a surprisingly high amount. Specifically, a signal was detected in the titration for ~1 IE1-defined transcriptional event, and based on the synthetic IE3 transcript standard, the amount of IE3 transcripts in 80 IE1-defined events was estimated to be ~400, that is, ~80% of the amount of IE1 transcripts. By contrast, transcripts of the early E-phase gene *M55/gB* (Fig. 6) and the late E-phase gene *m04*, encoding the immunosubversive protein gp34 (31) (data not shown), were below the detection limit of this highly sensitive assay.

Frequency of IE3 transcriptional events in TNF-induced latently infected lungs. With the new knowledge that IE3 transcripts are generated after induction with TNF-α and, moreover, in an amount comparable to the amount of IE1 transcripts, we went back to the piece-by-piece analysis of on-or-off transcription to determine the frequency of IE3 transcriptional splicing events (Fig. 7). Since the two transcripts are derived from a common IE1/3 precursor by differential splicing (29, 42), which generates either the IE1 or the IE3 mRNA from any single precursor molecule, the quantitative ratio between these two mRNA species is not necessarily 1:1 but is subject to splicing control. In addition, differential transcript stability can

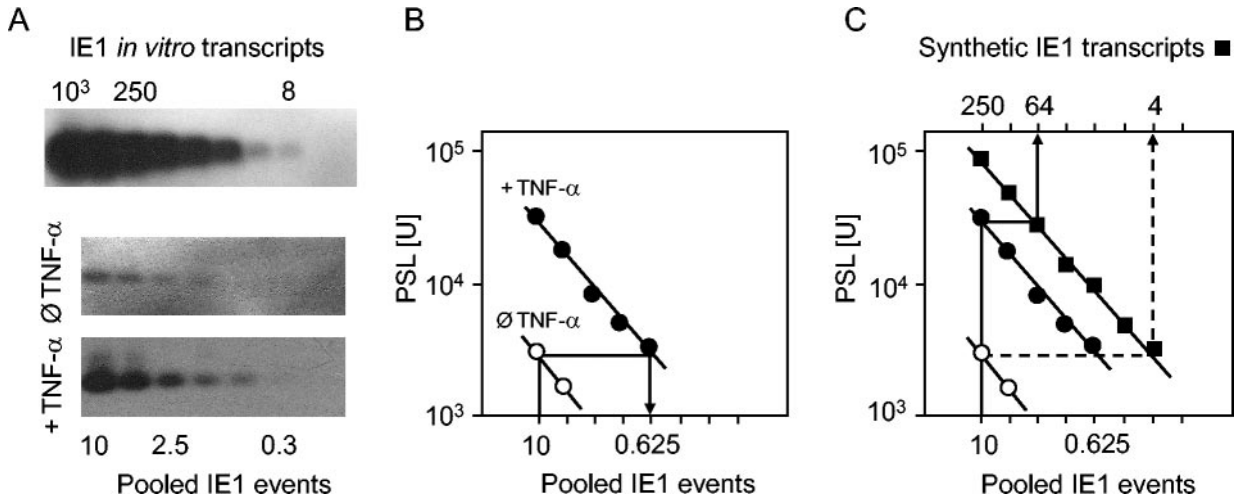

FIG. 5. Quantitation of the amount of IE1 transcripts. Aliquots of poly(A)$^+$ RNA from the IE1-positive lung pieces of the experiment shown in Fig. 4A were pooled separately for groups II.1 to II.5 and III.1 to III.5 representing basal (Ø TNF-α) and TNF-induced (1 μg of TNF-α) IE1 transcription, respectively. Serial dilutions were made, which contained 1% of the material that corresponded to defined numbers of transcriptional events, starting the titration series with 10 events. (A) Titration series of IE1 in vitro transcripts (top panel) and of lung-derived poly(A)$^+$ RNA from groups II and III normalized to the number of IE1 events (bottom panels). Shown are the Southern blot autoradiographs after hybridization with probe IE1-P. (B) Quantitation of radioactivity on the blots by phosphorimaging revealing a 16-fold difference in transcript amount between basal transcription (open circles) and TNF-induced transcription (closed circles). PSL, phosphostimulated luminescence in relative units. (C) Same graphs as those in panel B but with the standard curve (closed squares) included. As a reading example, a 1/100 fraction of 10 foci of the TNF-induced group III (closed circles) contains ~64 IE1 transcripts; that is, one IE1 focus in this group contains ~640 IE1 transcripts.

have an influence on the quantitative ratio observed in a snapshot experiment.

The original data are documented for individual mice III.1 and III.2 (Fig. 7A) and the frequency estimates based on the complete results for mice III.1 to III.5 are shown in Fig. 7C. As in Fig. 4A, ~200-ng aliquots representing 1/10 of the poly(A)$^+$ RNA yield of each piece were tested. It should be emphasized that the IE1 expression data in Fig. 4A and 7A were derived from independent aliquots. A comparison between the IE1 on-or-off patterns does not reveal a single mismatch, which documents a perfect reproducibility of the variegation patterns. This finding is in accordance with the quantitations made above. Specifically, a transcriptional event in group III was found to represent ~640 IE1 transcripts on average (Fig. 5), while the sensitivity analysis has shown that only ~80 IE1 transcripts are needed for detection in 10 out of 10 aliquots (Fig. 3). Thus, the patterns truly represent a quantal on-or-off phenomenon. It is worth noting that the IE1/3 precursor yields a 310-bp amplificate that encompasses the 122 bases of intron sequence between exons 3 and 4 (29) in the IE1-specific RT-PCR (33). This signal can be seen in pieces with high transcriptional activity, for instance, in piece 3 of mouse III.1 and piece 7 of mouse III.2 (Fig. 7A). The RNA nature of the template was verified with another sample aliquot by signal absence after omission of the RT step from the amplification reaction (C. O. Simon, unpublished data).

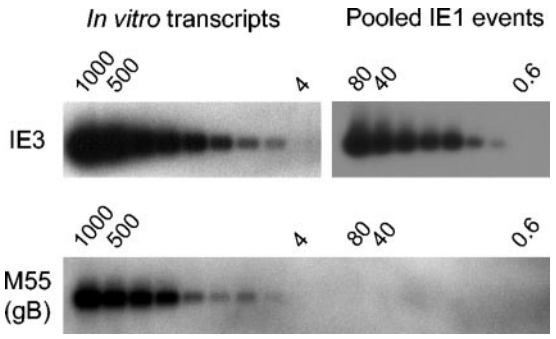

FIG. 6. Absence of M55/gB transcripts despite transactivator IE3 splicing. Aliquots of poly(A)$^+$ RNA from the 58 IE1-positive lung pieces of the TNF-induced group (mice III.1 to III.5 in Fig. 4A) were pooled. Serial dilutions were made, which contained 1% of the material that corresponded to defined numbers of transcriptional IE1 events, starting the titration series with 80 events. With a sample amount of ~1 μg of poly(A)$^+$ RNA in the RT-PCRs, the highest attainable assay sensitivity was reached. Standard titrations were performed with in vitro-synthesized IE3 and M55/gB transcripts, starting with 1,000 transcripts. Shown are Southern blot autoradiographs after hybridization with specific, γ-^{32}P-end-labeled probes. In the case of IE3-specific RT-PCR, a 229-bp cDNA amplificate was detected with probe IE3-P that was directed against the exon 3-exon 5 splicing junction of transcription unit *ie1/3*. In the case of M55/gB-specific RT-PCR, a 405-bp cDNA amplificate was detected with the internal probe gB-P.

Tissue pieces existed which, at the time of shock freezing, contained only IE1 but not IE3 transcripts, namely, pieces 8, 11, and 15 of mouse III.1 as well as pieces 14 and 15 of mouse III.2, whereas cases of isolated IE3 expression were not observed (Fig. 7A). Out of the 36 pieces, 17 were double negative, 14 were double positive, 5 were positive for IE1 only, and none were positive for IE3 only. When arranged in a 2-by-2 contingency table and analyzed by Fisher's exact probability test (37), these data give a P value of 0 for the null hypothesis of independent distribution (Fig. 7B). This statistical analysis supports the interpretation that IE3-positive foci also always contain IE1 transcripts (see below) (Fig. 9).

As a consequence of the existence of pieces containing IE1

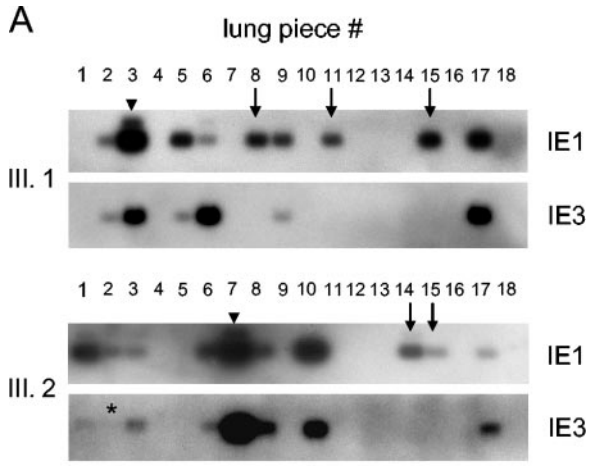

B

Observed

Assay for IE3 \ Assay for IE1	+	−	
+	14	0	14
−	5	17	22
	19	17	36

Expected

Assay for IE3 \ Assay for IE1	+	−	
+	7	7	14
−	12	10	22
	19	17	36

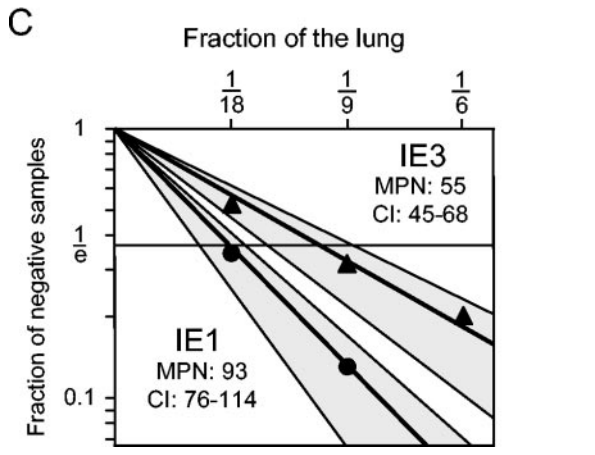

FIG. 7. Correlative patterns of IE1 and IE3 expression in pieces of latently infected lungs after induction with TNF-α. (A) Piece-by-piece RT-PCR analysis of the presence of IE1 and IE3 transcripts documented exemplarily for two mice of the TNF-induced group (mice III.1 and III.2, which had already been tested for IE1 in the experiment depicted in Fig. 4A). Note that IE1 expression was retested with an independent sample of the poly(A)$^+$ RNA to document pattern reproducibility. Shown are Southern blot autoradiographs after hybridization with probes IE1-P and IE3-P, respectively. The asterisk marks a faint signal that is visible on the original roentgen film. Arrows mark lung pieces that contain only IE1 transcripts. Arrowheads point to pieces of high expression for which the IE1/3 precursor RNA was detected in the form of an RT-dependent, 310-bp cDNA amplificate. (B) Contingency table analysis. To evaluate a possible correlation between IE1 and IE3 expression, the pattern data were organized in a 2-by-2 contingency table (observed pattern), and the null hypothesis of independent distribution (expected pattern in integers) was tested by applying Fisher's exact probability test. The expected value for double-positive pieces was 7.4. Null hypothesis was rejected with a *P* value of 0.000 that is <0.025 (one-tailed test for correlation). (C) Estimation of the frequencies of transcriptional foci based on the results from all 90 lung pieces derived from mice III.1 to III.5. Limiting dilution graphs show the linear regression lines with the 95% CI (shaded areas) for IE1 transcripts (closed circles) and IE3 transcripts (closed triangles). Based on the data from panel B, the frequency of IE3-positive foci can be interpreted as the frequency of double-positive foci.

but not IE3 transcripts, the cumulative frequency of IE3-positive events in mice III.1 to III.5 was lower than that of IE1-positive events, namely, 55 IE3 foci with a 95% confidence interval of 45 to 68 compared to 93 IE1 foci with a 95% confidence interval of 76 to 114 (Fig. 7C). As shown above, 80 IE1-defined transcriptional events contained ~500 IE1 transcripts and ~400 IE3 transcripts altogether. Considering the somewhat lower frequency of IE3 events, we conclude that the average amount of IE3 and IE1 transcripts was about the same in double-positive foci. This is different, though, if we look at individual lung tissue pieces (Fig. 7A). There were pieces in which IE1 transcripts predominated, for instance, in pieces 2, 3, 5, and 9 from mouse III.1 as well as in pieces 1, 2, and 6 from mouse III.2. On the other hand, IE3 transcripts predominated in piece 6 of mouse III.1 and in piece 17 of mouse III.2. The predominance of IE3 transcripts is remarkable in light of the finding that the amount of IE1 transcripts exceeds the amount of IE3 transcripts throughout the kinetics of productive mCMV infection of fibroblasts in cell culture (Simon, unpublished). Collectively, these expression patterns indicate that differences in IE1 and IE3 signal strengths do not merely reflect different assay sensitivity or transcript stability but represent real changes in the splicing program during an early stage of transcriptional reactivation.

TNF-induced MIE gene expression does not predispose for an enhanced virus recurrence. The transcription data have shown that the induction of MIE gene expression by TNF-α does not lead to the expression of E-phase genes downstream in the productive cycle. As a consequence, soluble TNF-α is not sufficient for inducing virus recurrence in an immunocompetent latently infected mouse. The central question was then whether the TNF-induced activated state increases the incidence of virus recurrence after application of a known trigger of reactivation, such as γ-rays (5, 51). To this end, mice with basal transcription and TNF-induced transcription, that is, mice of groups II and III, respectively, were exposed to total-body γ-irradiation. After 8 days, all 18 lung tissue pieces of each mouse were tested individually for the presence of infectious virus by a high-sensitivity assay of infectivity (35) that is based on centrifugal infection of permissive cell monolayers with tissue homogenate followed by the detection of IE1 transcripts after 3 days of focus expansion.

The mice of the two experimental groups were tested in pairs (mouse II.6 with mouse III.6, and so forth), that is, with 36 cultures per assay (Fig. 8). After completion of the results from three pairs, it was already statistically evident that there was no difference at all between the two groups, and therefore, we waived the remaining two pairs. With just 3 and 2 pieces scoring positive for infectivity out of 54 pieces tested for mice II.6 to II.8 and III.6 to III.8, respectively, the incidence of recurrence was generally very low, which relates to the low

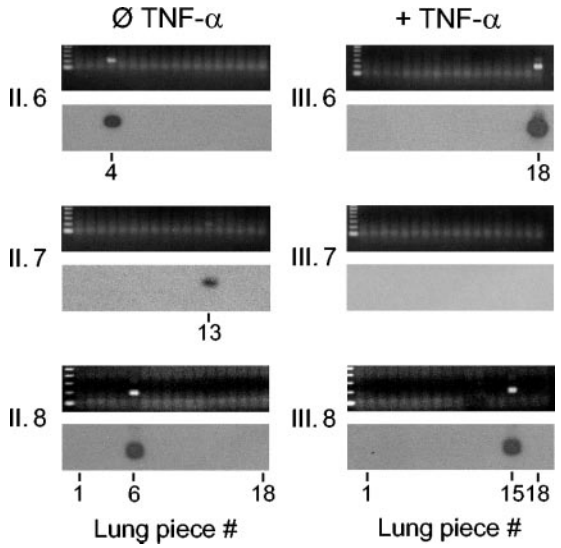

FIG. 8. Influence of TNF-α on the incidence of virus recurrence. At 24 h after i.v. infusion of saline (Ø TNF-α) and of 1 μg of recombinant murine TNF-α (+ TNF-α), mice of groups II and III, respectively, were immunosuppressed by total-body γ-irradiation with a dose of 6.5 Gy. On day 8, lung pieces were homogenized and tested individually for the presence of infectious virus by centrifugal infection of permissive indicator cell cultures followed by IE1-specific RT-PCR after 72 h of cultivation. Shown are the ethidium bromide-stained gels (top panels) and the corresponding Southern blot hybridizations with probe IE1-P (bottom panels). Frequency estimates (extrapolated to 90 pieces) were 6 (CI, 3 to 9) and 4 (CI, 2 to 7), respectively. As indicated by the overlap of the 95% CI, this is not a significant difference.

load of latent genomes in this group of latently infected BMT recipients.

In conclusion, while MIE gene expression and IE3 splicing are surely necessary early events in virus reactivation, they are not sufficient. Rather, downstream checkpoints provide further constraints that determine the incidence of γ-ray-induced virus recurrence.

DISCUSSION

The model for TNF-α function in the activation of CMV MIE gene expression proposes the induction of signaling cascades that activate the MIE enhancer through the binding of activated cellular transcription factors, specifically of NF-κB. Evidence in support of this sequence of events was provided first by Prösch and colleagues for hCMV MIE enhancer-promoter stimulation in a premonocytic cell line (49, 60). In support of an important role of the NF-κB pathway in productive hCMV replication, Caposio et al. (11) have recently shown that hCMV promotes its own replication by activating the IKK complex. Since the homologous MIE proteins UL122 (IE2) and M122 (IE3) of hCMV (22) and mCMV (4, 42), respectively, are essential transactivators of E gene expression in productive infection, it was reasonable to propose a decisive role for MIE enhancer stimulation through NF-κB binding for CMV reactivation from latency as well.

The predicted implication of the TNF-α/NF-κB signaling pathway in CMV reactivation was found to be in accordance with a coincidence of hCMV recurrence and elevated plasma TNF levels in septic patients (13), although this clinical study also revealed a coincidence with interleukin-6 and, if looked at, might have revealed a coincidence with any other parameter associated with sepsis. In an experimental model of intra-abdominal bacterial infection, Cook et al. (12) documented mCMV recurrence from latency under the stress conditions of sepsis. This recurrence is likely to have involved soluble and/or membrane-bound TNF-α, although many other factors associated with sepsis may have played a role. It therefore remained open to question whether soluble TNF-α on its own can induce CMV recurrence in vivo. At least as far as a crucial involvement of NF-κB is concerned, the original Prösch model for TNF-α function in the activation of CMV MIE gene expression (49) needs to be refined. While it is unquestioned that TNF-α induces NF-κB and that NF-κB has the potential to activate CMV MIE gene expression, a quite recent report by Benedict et al. (7) showed that the canonical NF-κB pathway of CMV MIE gene activation is dispensable for efficient CMV replication in cultured fibroblasts. Specifically, those authors knocked out all four NF-κB binding sites in the hCMV enhancer by site-directed mutagenesis with no consequence for the replication of an mCMV enhancer swap mutant in which the mCMV enhancer was replaced by the NF-κB site-deficient hCMV enhancer. This notable result may indicate that the constitutive MIE enhancer-promoter activity initiates a MIE gene expression that is sufficient for viral growth. Alternatively, it may indicate a robustness of the regulation due to redundancy in the enhancer-activating signaling pathways. However, as already discussed by Benedict et al. (7), the regulation of MIE gene expression in dividing, fully permissive cells in cell culture is not necessarily identical to the signaling requirements for the reactivation of silenced, latent genomes in contact-inhibited host tissue cells. Open and closed chromatin structures, respectively, are likely to be a key difference (see below).

Hummel et al. (26) have shown that in vivo induction of mCMV IE1 gene expression by TNF-α in latently infected lungs is associated with the activation of cellular transcription factors NF-κB as well as AP1. The mCMV enhancer encompasses multiple tandem repeats of NF-κB and AP1 binding sites (14), and through binding to TNF receptors, TNF-α activates AP1 along the TRADD-TRAF2-MEKK1-MKK7-JNK pathway (for a review, see reference 2). Since Hummel et al. did not detect IE1 transcripts under conditions of selective induction of either NF-κB (in the kidney after TNF-α was administered i.v.) or AP1 (in syngeneic kidney transplants), those authors favored the interpretation that both are required for the in vivo reactivation of IE1 gene expression (25, 26).

Previous studies on mCMV latency in the lungs have revealed a low basal frequency of MIE transcription from the *ie1/3* transcription unit as well as from the *ie2* gene but an absence of spliced IE3 mRNA (19, 33) encoding the essential transactivator of downstream E gene expression (4). Accordingly, M55/gB transcripts and infectious virus were absent too. This finding explained the maintenance of latency in the presence of MIE transcription and identified IE3 splicing as a molecular checkpoint of latency beyond enhancer regulation and MIE gene transcription initiation. Here, we used this well-established experimental model to quantitate the inducing effect of TNF-α on MIE gene expression in latently infected

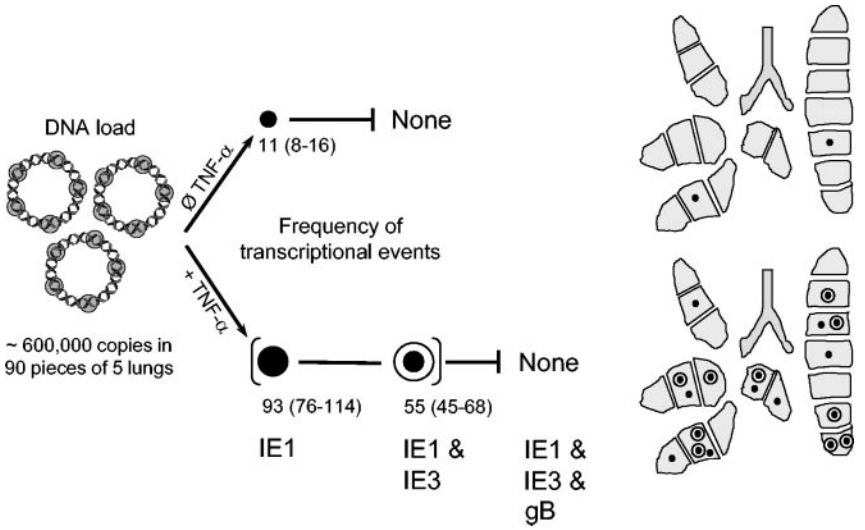

FIG. 9. Summary of results for latency-associated transcription. Data for TNF-α refer to the dose of 1 μg (+ TNF-α). Frequency estimates for transcriptional events or foci refer to 90 lung pieces of five mice and are given as MPN (95% CI). Latent viral chromosomes are symbolized as coils. The difference between the two groups is illustrated by topographical lung maps showing the types (IE1, closed circle; IE1 and IE3, closed circle within open circle), numbers, and distribution of foci in statistically representative lungs. For this, the fraction of pieces containing n (n = 0, 1, 2, 3, or 4) foci, $F(n)$, was first calculated separately for IE1 and IE3, and the distribution of foci was then defined under the premise that IE3 foci (open circles) coincide with IE1 foci (closed circles). See the legend of Fig. 7B for the justification of this premise. Note that individual lungs with a transcriptional activity that is higher than the representative transcriptional activity contained a maximum of four foci in a piece (data not shown).

lungs and to answer the question of whether enhanced MIE gene expression can drive the productive viral cycle all the way through to the release of infectious virus, as has been proposed by previous studies on the role of TNF-α in CMV reactivation.

Basal transcriptional activity in latently infected lungs. For an easier overview and discussion, our data on latency-associated transcription are summarized in Fig. 9. As a starting point, the number of latent viral genomes was determined to be ~2,000 copies per 10^6 lung cells, which equals ~600,000 copies per five lungs. In the absence of TNF-α, basal activity from the MIE *ie1/3* transcription unit occurred in a frequency of 11 (8 to 16) transcriptional events per five lungs.

The number of viral genomes per latently infected lung cell is not precisely known, although an estimate of 1 to 8 has been made for differentiation-dependent conditionally permissive granulocyte-macrophage progenitors, a cell culture model of hCMV latency (55). It is also unknown whether such an event or focus represents transcription from one or more genomes. Based on the low average number of transcripts per focus, namely, ~40, it is conceivable that just one active genome in a single latently infected cell defines a transcriptional focus. Therefore, the number of foci would represent the minimum number of latently infected cells that contain IE1 transcripts. With this conjecture, only ~1 out of 60,000 latent viral genomes was transcriptionally active at the MIE locus. The very low frequency of IE1 foci combined with the low amount of transcripts per focus and the dependence on the latent template load in tissue explains why the expression of *ie1* during latency was not observed by all investigators (26) and remained controversial for a long time (for a discussion, see reference 25). It is evident that our strategy to test individual pieces of the lungs and to use purified poly(A)$^+$ RNA in an optimized RT-PCR facilitated the detection of this phenomenon, which has now been reproduced repeatedly (references 19, 33, and 34 and this report). The finding that only a very minor proportion of the latent viral genomes is transcriptionally active in vivo is in accordance with the detection of hCMV latency-associated MIE region transcripts (32) in only a small proportion of viral DNA-positive granulocyte-macrophage progenitors in cell culture (55). This phenomenon, also known as variegation, is reminiscent of the expression of transgenes, which are present in all cells but are silenced or active depending on a closed or open chromatin structure, respectively (16; for more discussion, see reference 19). Although the CMV genome persists as an episome, at least as far as what has been learned for hCMV from CD14-positive hematopoietic cells (8) and embryonal carcinoma cells (41), it most likely exists in a chromatin-like structure (41, 43). Specifically, in nonpermissive monocytes, the hCMV MIEP associates with heterochromatin protein 1, a chromosomal protein implicated in gene silencing, while it associates with acetylated histones in permissive cells (43). Along the same line of evidence, inhibition of histone deacetylase was found to reactivate MIE gene expression as well as the release of infectious virus in otherwise nonpermissive embryonal carcinoma cells (41). We propose that latent mCMV in a host organ is mostly tightly silenced and that the low frequency of IE1 transcription observed by us in latently infected lungs reflects very rare events of desilencing at the MIE locus, putatively by histone acetylation or prevention of deacetylation. While the occurrence of this rare event can be described by a discrete random function (19), this should not be misinterpreted as being a molecularly unsolicited, spontaneous event. Rather, a reactivating signal may by itself occur randomly as a sort of "noise" signal. It should be emphasized that our analyses represent snapshots by shock freezing. Although not testable on-line in an organ of a living being, we hypoth-

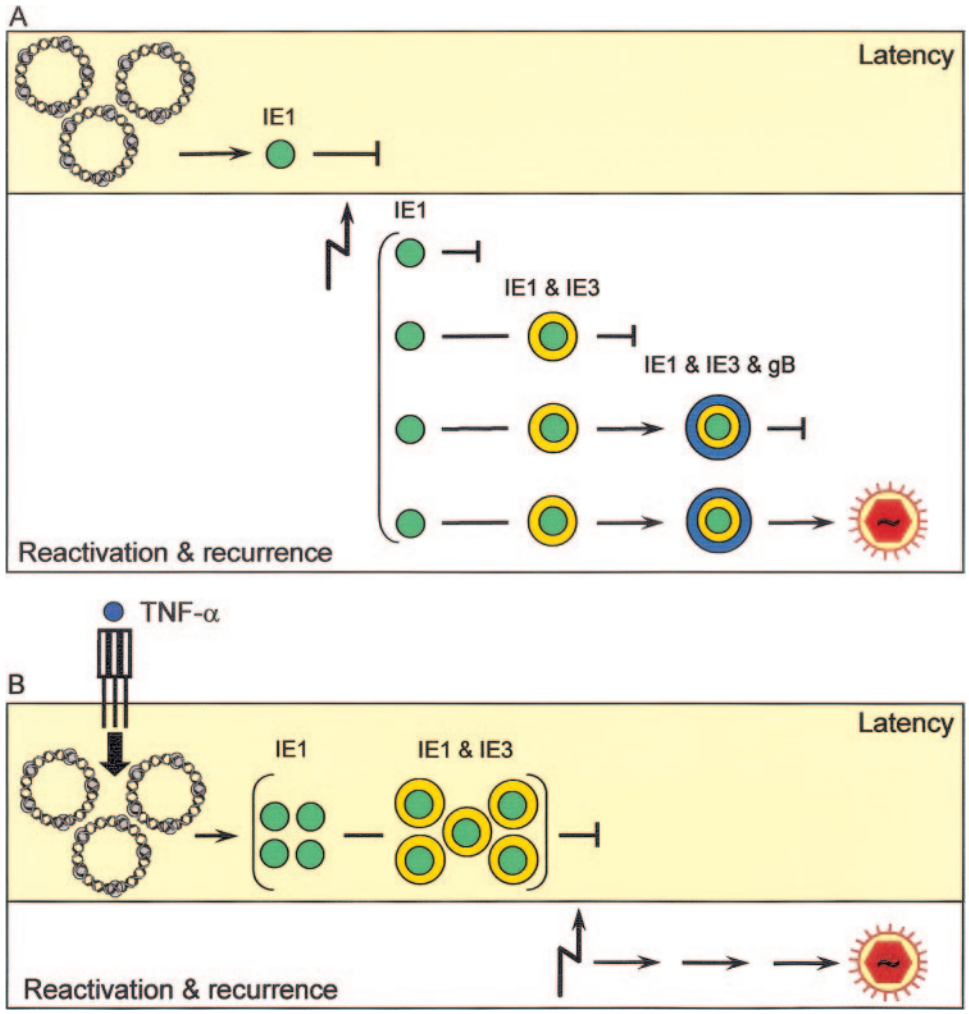

FIG. 10. Models of CMV latency and reactivation. (A) Multistep model of CMV reactivation, modified from a model by Kurz and Reddehase (34). Latent viral chromosomes are symbolized as coils. During latency, transcription is arrested at IE1 (closed green circles). After induction of reactivation by γ-rays, some foci of transcription remain arrested at IE1, others contain spliced IE3 transcripts (yellow shell), yet others proceed to M55/gB transcription (blue shell), and only few complete the productive cycle and release infectious virus (virion symbol [red]). (B) Role of TNF-α (this report). Through the NF-κB/AP1 signaling pathways, TNF-α enhances MIE gene transcription by >100-fold and promotes differential splicing, which leads to IE1 foci and IE1 and IE3 foci in a ratio of ~4/5. This activated state, however, does not predispose for an increased incidence of virus recurrence after γ-ray-induced reactivation. It is proposed that multiple checkpoints downstream in the productive cycle of gene expression, putatively defined by random patterns of locally closed and open chromatin-like structures, are rate limiting for recurrence.

esize that the observed random patterns of transcription in the lungs are not static but that MIE transcription, if seen in a time lapse, is switched on and off. It is worth noting that latency-associated transcription may differ between different tissues, probably due to specific gene silencing environments. Specifically, Kercher and Mitchell (30) described the presence of mCMV IE1 and gH transcripts in latently infected ocular tissue. As shown recently for the myeloid progenitor cell culture model of hCMV latency, latency-associated viral transcription has an impact on cellular gene expression proposed to generate an environment that sustains latent infection (27, 56).

Transcriptional reactivation promoted by TNF-α. One candidate for the discussed noise signaling in the lungs was TNF-α, because of its known impact on MIE gene expression (discussed above) and because some activation of producer cells such as alveolar macrophages is always to be expected in an organ that is particularly exposed to environmental antigens due to its huge inner surface. By administering soluble TNF-α experimentally, we have shown here a dose-dependent increase in the frequency of transcriptional events at the MIE locus, namely, up to ~8-fold at the highest nonlethal dose, accompanied by a ~16-fold increase in the amount of IE1 transcripts per focus. Nonetheless, with ~100 transcriptional events per 600,000 latent genomes, by far most of the latent viral genomes remained silenced. This result clearly tells us that TNF-α is not the inductor of MIE reactivation permissiveness but only induces MIE gene expression from already permissive genomes. As discussed above, an open chromatin structure at the MIE locus is likely a key condition for MIE gene expression. From the literature, we are not aware of a direct influence of TNF-α on histone acetylation, but there is evidence to suggest that acetylation has an enhancing influence

on TNF-α/NF-κB- or TNF-α/AP1-mediated transcription (1). We propose that the frequencies observed with TNF-α more closely represent the number of latently infected cells that are permissive to reactivation of MIE gene expression and that the role of TNF-α is to enhance MIE gene expression from permissive, desilenced viral genomes. As shown by Ghazal et al. (17), basal activity of the MIE1/3 promoter in an enhancerless mCMV mutant is insufficient for in vivo virus replication. Therefore, to become visible as a transcriptional focus in the assay, a latently infected cell must contain a viral genome(s) with an open chromatin structure at the MIE locus, which is a prerequisite for transcription, and the MIE enhancer must be sufficiently activated by transcription factors, namely, by NF-κB and/or AP1 in the case of signaling through TNF receptors, in order to generate a detectable number of transcripts. This latter condition appears to be TNF-α dose dependent.

In previous work on the basal MIE gene activity in latently infected lungs, the absence of spliced IE3 transcripts was a molecular hallmark of mCMV latency, and differential splicing of the IE1/3 precursor was discussed as a checkpoint of latency, the second checkpoint after enhancer-driven *ie1/3* transcription initiation (33, 34). The generation of IE3 mRNA after induction with TNF-α is a major new finding. It is of course a critical question whether TNF-α/NF-κB or TNF-α/AP1 signaling just improved the detectability of IE3 mRNA by an enhancement of the *ie1/3* transcription rate or whether it mediated a qualitative change in the splicing program. As shown in Fig. 7, detection of IE3 mRNA was not linked to high expression of IE1, which is also in accordance with previous data on a change in the splicing program after γ-ray-induced virus reactivation (33). We therefore believe in a qualitative effect. The mechanism by which TNF-α influences differential RNA splicing, however, is an open question.

Refined model of virus reactivation and recurrence. It is notable that presence of IE3 transcripts did not lead to transactivation of the full E-phase program, shown here representatively for the essential gene *M55/gB*. Thus, TNF-α did not induce recurrence of infectious virus in the immunocompetent host. This finding is in accordance with the work by Hummel et al. (26), who proposed a two-step model of virus reactivation consisting of MIE gene activation by inflammatory cytokines, specifically of TNF-α, followed by immunosuppression. The two-step model thus predicted that a combination of TNF-α and removal of immune control by γ-irradiation (51) or depletion of immune cell subsets (47) would increase the incidence of recurrence. As shown in Fig. 8, this was not the case. Instead, these data are better explained by the multistep model (Fig. 10A) proposed previously by Kurz and Reddehase (34). This model was based on the experimental finding that γ-irradiation leads to virus recurrence in only a small proportion of reactivation foci in the lungs. Some foci remained at the stage of selective IE1 expression, others switched to IE3 splicing, yet others moved on to the expression of *M55/gB*, and only a few were successful in completing the productive cycle (34). Therefore, in line with the data reported here, detection of IE3 transcripts did not indicate full reactivation. One could discuss that posttranscriptional control in these foci might have prevented the synthesis of the transactivating IE3 protein. However, the simultaneous existence of M55/gB transcripts in other reactivation foci in the same lungs implies synthesis of and effective transactivation by the IE3 protein. Our refined model (Fig. 10B) includes the information that TNF-α increases the number of IE1 foci and promotes IE3 splicing but that transcriptional reactivation does not proceed to the expression of M55/gB in the lungs of an immunocompetent host.

Notably, against previous views and predictions, the incidence of virus recurrence after the removal of immune control was not enhanced by a preceding induction with TNF-α. This finding may relate to a dual role of this inflammatory cytokine in the regulation of CMV replication. While TNF-α kick starts the viral transcriptional program due to its enhancing effect on MIE gene expression, it can simultaneously induce an antiviral state that becomes effective later in the productive cycle. Specifically, in combination with gamma interferon, TNF-α inhibits M55/gB expression and nucleocapsid maturation (39).

Based on previous data on reactivation-associated viral transcription (34), we prefer the hypothesis that one or more checkpoints downstream of MIE gene expression are rate limiting for recurrence. The nature of these proposed checkpoints is undefined. One idea is that for full reactivation, the supercoiled latent viral chromosome (8, 41, 43), which in stretched length is equivalent to ~1,150 nucleosome distances, must be simultaneously open at all essential genes, not just at the MIE locus. This condition is likely to be met by the induction of proliferation and differentiation of latently infected cells in the various cell culture and tissue explantation systems as well as transplantation systems reported (for reviews, see references 25, 28, and 52), after allogeneic stimulation (57), and by combined action of multiple mediators in sepsis (12, 13).

This model predicts that the maintenance of a closed viral chromatin structure at any single essential gene anywhere in the viral gene expression program can prevent recurrence of infectious virus. Clearly, a random pattern of locally closed and open portions of viral chromatin explains the "patchwork pattern" of transcriptional reactivation observed by Kurz and Reddehase (34) as well as the data presented here. As a consequence, if this model applies, it is pointless to search for additional specific molecular checkpoints of latency.

ACKNOWLEDGMENTS

We thank Michael M. Abecassis, Northwestern University Medical School, Chicago, Ill., for sharing the protocol for in vivo TNF application with us before publication.

Support was provided by a grant to N.K.A.G. and M.J.R. by the Deutsche Forschungsgemeinschaft, Sonderforschungsbereich 490, individual project B1 "Immune control of latent cytomegalovirus infection."

REFERENCES

1. **Adam, E., V. Quivy, F. Bex, A. Chariot, Y. Collette, C. Vanhulle, S. Schoonbroodt, V. Goffin, T. L. Nguyen, G. Gloire, G. Carrard, B. Friguet, Y. De Launoit, A. Burny, V. Bours, J. Piette, and C. Van Lint.** 2003. Potentiation of tumor necrosis factor-induced NF-κB activation by deacetylase inhibitors is associated with a delayed cytoplasmic reappearance of IκBα. Mol. Cell. Biol. **23:**6200–6209.
2. **Aggarwal, B. B.** 2003. Signalling pathways of the TNF superfamily: a double-edged sword. Nat. Rev. Immunol. **3:**745–756.
3. **Alterio de Goss, M., R. Holtappels, H.-P. Steffens, J. Podlech, P. Angele, L. Dreher, D. Thomas, and M. J. Reddehase.** 1998. Control of cytomegalovirus in bone marrow transplantation chimeras lacking the prevailing antigen-presenting molecule in recipient tissues rests primarily on recipient-derived CD8 T cells. J. Virol. **72:**7733–7744.

4. **Angulo, A., P. Ghazal, and M. Messerle.** 2000. The major immediate-early gene *ie3* of mouse cytomegalovirus is essential for viral growth. J. Virol. **74:**11129–11136.
5. **Balthesen, M., M. Messerle, and M. J. Reddehase.** 1993. Lungs are a major organ site of cytomegalovirus latency and recurrence. J. Virol. **67:**5360–5366.
6. **Barry, S. M., M. A. Johnson, and G. Janossy.** 2000. Cytopathology or immunopathology? The puzzle of cytomegalovirus pneumonitis revisited. Bone Marrow Transplant. **26:**591–597.
7. **Benedict, C. A., A. Angulo, G. Patterson, S. Ha, H. Huang, M. Messerle, C. F. Ware, and P. Ghazal.** 2004. Neutrality of the canonical NF-κB-dependent pathway for human and murine cytomegalovirus transcription and replication in vitro. J. Virol. **78:**741–750.
8. **Bolovan-Fritts, C. A., E. S. Mocarski, and J. A. Wiedeman.** 1999. Peripheral blood $CD14^+$ cells from healthy subjects carry a circular conformation of latent cytomegalovirus genome. Blood **93:**394–398.
9. **Boshart, M., F. Weber, G. Jahn, K. Dorsch-Häsler, B. Fleckenstein, and W. Schaffner.** 1985. A very strong enhancer is located upstream of an immediate early gene of human cytomegalovirus. Cell **41:**521–530.
10. **Brouckaert, P., C. Libert, B. Everaerdt, and W. Fiers.** 1992. Selective species specificity of tumor necrosis factor for toxicity in the mouse. Lymphokine Cytokine Res. **11:**193–196.
11. **Caposio, P., M. Dreano, G. Garotta, G. Gribaudo, and S. Landolfo.** 2004. Human cytomegalovirus stimulates cellular IKK2 activity and requires the enzyme for productive replication. J. Virol. **78:**3190–3195.
12. **Cook, C. H., Y. Zhang, B. J. McGuinness, M. C. Lahm, D. D. Sedmak, and R. M. Ferguson.** 2002. Intra-abdominal bacterial infection reactivates latent pulmonary cytomegalovirus in immunocompetent mice. J. Infect. Dis. **185:** 1395–1400.
13. **Döcke, W. D., S. Prösch, E. Fietze, V. Kimel, H. Zuckermann, C. Klug, U. Syrbe, D. H. Krüger, R. von Baehr, and H. D. Volk.** 1994. Cytomegalovirus reactivation and tumour necrosis factor. Lancet **343:**268–269.
14. **Dorsch-Häsler, K., G. M. Keil, F. Weber, M. Jasin, W. Schaffner, and U. H. Koszinowski.** 1985. A long and complex enhancer activates transcription of the gene coding for the highly abundant immediate early mRNA in murine cytomegalovirus. Proc. Natl. Acad. Sci. USA **82:**8325–8329.
15. **Fazekas de St. Groth, S.** 1982. The evaluation of limiting dilution assays. J. Immunol. Methods **49:**R11–R23.
16. **Fiering, S., E. Whitelaw, and D. I. K. Martin.** 2000. To be or not to be active: the stochastic nature of enhancer action. Bioessays **22:**381–387.
17. **Ghazal, P., M. Messerle, K. Osborn, and A. Angulo.** 2003. An essential role of the enhancer for murine cytomegalovirus in vivo growth and pathogenesis. J. Virol. **77:**3217–3228.
18. **Ghazal, P., and J. A. Nelson.** 1993. Transcription factors and viral regulatory proteins as potential mediators of human cytomegalovirus pathogenesis, p. 360–383. *In* Y. Becker, G. Darai, and E. S. Huang (ed.), Molecular aspects of human cytomegalovirus diseases. Springer Verlag Publishers, Heidelberg, Germany.
19. **Grzimek, N. K. A., D. Dreis, S. Schmalz, and M. J. Reddehase.** 2001. Random, asynchronous, and asymmetric transcriptional activity of enhancer-flanking major immediate-early genes *ie1/3* and *ie2* during murine cytomegalovirus latency in the lungs. J. Virol. **75:**2692–2705.
20. **Gubbay, J., J. Collignon, P. Koopman, B. Capel, A. Economou, A. Münsterberg, N. Vivian, P. Goodfellow, and R. Lovell-Badge.** 1990. A gene mapping to the sex-determining region of the mouse Y chromosome is a member of a novel family of embryonically expressed genes. Nature **346:**245–250.
21. **Henry, S. C., and J. D. Hamilton.** 1993. Detection of murine cytomegalovirus immediate early 1 transcripts in the spleens of latently infected mice. J. Infect. Dis. **167:**950–954.
22. **Hermiston, T. W., C. L. Malone, P. R. Witte, and M. F. Stinski.** 1987. Identification and characterization of the human cytomegalovirus immediate-early region 2 gene that stimulates gene expression from an inducible promoter. J. Virol. **61:**3214–3221.
23. **Holtappels, R., M.-F. Pahl-Seibert, D. Thomas, and M. J. Reddehase.** 2000. Enrichment of immediate-early 1 (*m123*/pp89) peptide-specific CD8 T cells in a pulmonary $CD62L^{lo}$ memory-effector cell pool during latent murine cytomegalovirus infection of the lungs. J. Virol. **74:**11495–11503.
24. **Holtappels, R., J. Podlech, G. Geginat, H.-P. Steffens, D. Thomas, and M. J. Reddehase.** 1998. Control of murine cytomegalovirus in the lungs: relative but not absolute immunodominance of the immediate-early 1 nonapeptide during the antiviral cytolytic T-lymphocyte response in pulmonary infiltrates. J. Virol. **72:**7201–7212.
25. **Hummel, M., and M. M. Abecassis.** 2002. A model for reactivation of CMV from latency. J. Clin. Virol. **25:**S123–S136.
26. **Hummel, M., Z. Zhang, S. Yan, I. Deplaen, P. Golia, T. Varghese, G. Thomas, and M. I. Abecassis.** 2001. Allogeneic transplantation induces expression of cytomegalovirus immediate-early genes in vivo: a model for reactivation from latency. J. Virol. **75:**4814–4822.
27. **Jenkins, C., A. Abendroth, and B. Slobedman.** 2004. A novel viral transcript with homology to human interleukin-10 is expressed during latent human cytomegalovirus infection. J. Virol. **78:**1440–1447.
28. **Jordan, M. C.** 1983. Latent infection and the elusive cytomegalovirus. Rev. Infect. Dis. **5:**205–215.
29. **Keil, G. M., A. Ebeling-Keil, and U. H. Koszinowski.** 1987. Sequence and structural organization of murine cytomegalovirus immediate-early gene 1. J. Virol. **61:**1901–1908.
30. **Kercher, L., and B. M. Mitchell.** 2002. Persisting murine cytomegalovirus can reactivate and has unique transcriptional activity in ocular tissue. J. Virol. **76:**9165–9175.
31. **Kleijnen, M. F., J. B. Huppa, P. Lucin, S. Mukherjee, H. Farrell, A. E. Campbell, U. H. Koszinowski, A. B. Hill, and H. L. Ploegh.** 1997. A mouse cytomegalovirus glycoprotein, gp34, forms a complex with folded class I MHC molecules in the ER which is not retained but is transported to the cell surface. EMBO J. **16:**685–694.
32. **Kondo, K., J. Xu, and E. S. Mocarski.** 1996. Human cytomegalovirus latent gene expression in granulocyte-macrophage progenitors in culture and in seropositive individuals. Proc. Natl. Acad. Sci. USA **93:**11137–11142.
33. **Kurz, S. K., M. Rapp, H.-P. Steffens, N. K. A. Grzimek, S. Schmalz, and M. J. Reddehase.** 1999. Focal transcriptional activity of murine cytomegalovirus during latency in the lungs. J. Virol. **73:**482–494.
34. **Kurz, S. K., and M. J. Reddehase.** 1999. Patchwork pattern of transcriptional reactivation in the lungs indicates sequential checkpoints in the transition from murine cytomegalovirus latency to recurrence. J. Virol. **73:**8612–8622.
35. **Kurz, S. K., H.-P. Steffens, A. Mayer, J. R. Harris, and M. J. Reddehase.** 1997. Latency versus persistence or intermittent recurrences: evidence for a latent state of murine cytomegalovirus in the lungs. J. Virol. **71:**2980–2987.
36. **Lefkovits, I., and H. Waldman.** 1979. Limiting dilution analysis of cells in the immune system, p. 38–82. Cambridge University Press, Cambridge, England.
37. **Lefkovits, I., and H. Waldman.** 1979. Limiting dilution analysis of cells in the immune system, p. 95–100. Cambridge University Press, Cambridge, England.
38. **Ljungman, P.** 2002. Beta-herpesvirus challenges in the transplant recipient. J. Infect. Dis. **186(Suppl. 1):**S99–S109.
39. **Lucin, P., S. Jonjic, M. Messerle, B. Polic, H. Hengel, and U. H. Koszinowski.** 1994. Late phase inhibition of murine cytomegalovirus replication by synergistic action of interferon-gamma and tumor necrosis factor. J. Gen. Virol. **75:**101–110.
40. **Mangin, M., K. Ikeda, and A. E. Broadus.** 1990. Structure of the mouse gene encoding parathyroid hormone-related peptide. Gene **95:**195–202.
41. **Meier, J. L.** 2001. Reactivation of the human cytomegalovirus major immediate-early regulatory region and viral replication in embryonal NTera2 cells: role of trichostatin A, retinoic acid, and deletion of the 21-base-pair repeats and modulator. J. Virol. **75:**1581–1593.
42. **Messerle, M., B. Bühler, G. M. Keil, and U. H. Koszinowski.** 1992. Structural organization, expression, and functional characterization of the murine cytomegalovirus immediate-early gene 3. J. Virol. **66:**27–36.
43. **Murphy, J. C., W. Fischle, E. Verdin, and J. H. Sinclair.** 2002. Control of cytomegalovirus lytic gene expression by histone acetylation. EMBO J. **21:** 1112–1120.
44. **Pass, R. F.** 2001. Cytomegalovirus, p. 2675–2705. *In* D. M. Knipe and P. M. Howley (ed.), Fields virology, 4th ed. Lippincott Williams & Wilkins, Philadelphia, Pa.
45. **Podlech, J., R. Holtappels, N. K. A. Grzimek, and M. J. Reddehase.** 2002. Animal models: murine cytomegalovirus, p. 493–525. *In* S. H. E. Kaufmann and D. Kabelitz (ed.), Methods in microbiology, 2nd ed., vol. 32. Immunology of infection. Academic Press, San Diego, Calif.
46. **Podlech, J., R. Holtappels, M.-F. Pahl-Seibert, H.-P. Steffens, and M. J. Reddehase.** 2000. Murine model of interstitial cytomegalovirus pneumonia in syngeneic bone marrow transplantation: persistence of protective pulmonary CD8-T-cell infiltrates after clearance of acute infection. J. Virol. **74:** 7496–7507.
47. **Polic, B., H. Hengel, A. Krmpotic, J. Trgovcich, I. Pavic, P. Lucin, S. Jonjic, and U. H. Koszinowski.** 1998. Hierarchical and redundant lymphocyte subset control precludes cytomegalovirus replication during latent infection. J. Exp. Med. **21:**1047–1054.
48. **Popkin, D. L. and H. W. Virgin IV.** 2003. Murine cytomegalovirus infection inhibits tumor necrosis factor alpha responses in primary macrophages. J. Virol. **77:**10125–10130.
49. **Prösch, S., K. Staak, J. Stein, C. Liebenthal, T. Stamminger, H.-D. Volk, and D. H. Krüger.** 1995. Stimulation of the human cytomegalovirus IE enhancer/promoter in HL-60 cells by TNFα is mediated via induction of NF-κB. Virology **208:**197–206.
50. **Rawlinson, W. D., H. E. Farrell, and B. G. Barrell.** 1996. Analysis of the complete DNA sequence of murine cytomegalovirus. J. Virol. **70:**8833–8849.
51. **Reddehase, M. J., M. Balthesen, M. Rapp, S. Jonjic, I. Pavic, and U. H. Koszinowski.** 1994. The conditions of primary infection define the load of latent viral genome in organs and the risk of recurrent cytomegalovirus disease. J. Exp. Med. **179:**185–193.
52. **Reddehase, M. J., J. Podlech, and N. K. A. Grzimek.** 2002. Mouse models of cytomegalovirus latency: overview. J. Clin. Virol. **25:**S23–S36.
53. **Reddehase, M. J., F. Weiland, K. Münch, S. Jonjic, A. Lüske, and U. H. Koszinowski.** 1985. Interstitial murine cytomegalovirus pneumonia after irradiation: characterization of cells that limit viral replication during established infection of the lungs. J. Virol. **55:**264–273.

54. **Riddell, S. R.** 1995. Pathogenesis of cytomegalovirus pneumonia in immunocompromised hosts. Semin. Respir. Infect. **10:**199–208.
55. **Slobedman, B., and E. S. Mocarski.** 1999. Quantitative analysis of latent human cytomegalovirus. J. Virol. **73:**4806–4812.
56. **Slobedman, B., J. L. Stern, A. L. Cunningham, A. Abendroth, D. A. Abate, and E. S. Mocarski.** 2004. Impact of human cytomegalovirus latent infection on myeloid progenitor cell gene expression. J. Virol. **78:**4054–4062.
57. **Soderberg-Naucler, C., K. N. Fish, and J. A. Nelson.** 1997. Reactivation of latent human cytomegalovirus by allogeneic stimulation of blood cells from healthy donors. Cell **91:**119–126.
58. **Spector, D. H.** 1996. Activation and regulation of human cytomegalovirus early genes. Intervirology **39:**361–377.
59. **Steffens, H.-P., S. Kurz, R. Holtappels, and M. J. Reddehase.** 1998. Preemptive CD8 T-cell immunotherapy of acute cytomegalovirus infection prevents lethal disease, limits the burden of latent viral genomes, and reduces the risk of virus recurrence. J. Virol. **72:**1797–1804.
60. **Stein, J., H. D. Volk, C. Liebenthal, D. H. Krüger, and S. Prösch.** 1993. Tumour necrosis factor alpha stimulates the activity of the human cytomegalovirus major immediate early enhancer/promoter in immature monocytic cells. J. Gen. Virol. **74:**2333–2338.
61. **Taswell, C.** 1981. Limiting dilution assays for the determination of immunocompetent cell frequencies. I. Data analysis. J. Immunol. **126:**1614–1619.
62. **Yuhasz, S. A., V. B. Dissette, M. L. Cook, and J. G. Stevens.** 1994. Murine cytomegalovirus is present in both chronic active and latent states in persistently infected mice. Virology **202:**272–280.